

Influence of Thermo-mechanical Processing Parameters on Grain Boundary Character Distribution Evolution of Cold-Rolled Ni-Based Superalloy

Zhang Hongbin¹, Zhou Haiping¹, Zhang Chengcai¹, Han Baokun¹, Gao Kuidong¹,
Li Huiping¹, Qin Shengxue¹, Liu Jie¹, Wang Yan¹, Zhang Peng²

¹ Shandong University of Science and Technology, Qingdao 266590, China; ² Fushun Special Steel Co., Ltd, Fushun 113000, China

Abstract: The influence of thermo-mechanical processing (TMP) parameters on the grain boundary character distribution evolution of cold-rolled Ni-based superalloy was studied. Results show that during annealing treatment, growth accident model is considered to be the main mechanism for the formation of new $\Sigma 3$ boundaries in the static recrystallization (SRX) grains. With increasing the annealing time and temperature, there is more time for grain boundary migration and the grain boundary migration is faster at higher annealing temperatures, which can stimulate the formation of $\Sigma 3$ boundaries by increasing the frequency of growth accidents. In addition, the fraction of $\Sigma 3$ boundaries decreases firstly with increasing the strain, and then increases again. At the strains of 0.1 and 0.7, the fractions of $\Sigma 3$ boundaries reach around 60%, which is related to the well development of large grain-clusters. Besides, the evolution of $\Sigma 1$ boundaries, coherent $\Sigma 3$ boundaries, incoherent $\Sigma 3$ boundaries, $\Sigma 9$ boundaries, $\Sigma 27$ boundaries, and random boundaries were also analyzed.

Key words: Ni-based superalloy; grain boundary character distribution; CSL boundary; thermo-mechanical processing

Ni-based superalloys have been widely applied in the aerospace, chemical and petrochemical industrial fields, owing to their superior mechanical properties and corrosion resistance under the high temperature conditions [1]. With the rapid development of these fields, the working condition of Ni-based superalloy has become more and more severe, while the prolonged service life and improved performance are also demanded [2, 3]. However, intergranular corrosion is one of the most serious problems for Ni-based superalloy in the aggressive environments, which can directly affect the safe service. In this work, further improvement of the resistance to intergranular failure for Ni-based superalloy should be considered.

At present, grain boundary engineering (GBE) has been demonstrated as an effective approach to improve the resistance to intergranular corrosion for Ni-based superalloy [4, 5]. Meanwhile, the improvement of corrosion resistance by

GBE involves increasing the fraction of low- Σ ($\Sigma \leq 29$) coincident site lattice (CSL) boundaries, and disrupting the random grain boundary network. It should be noted that the low- Σ CSL boundaries are known as special boundaries, owing to their low distortion of atomic bonds, low interface energy, and high resistance to intergranular damage [5]. In GBE, thermo-mechanical processing (TMP) has been commonly used to increase the fraction of low- Σ CSL boundaries, mainly through cold rolling and subsequent annealing [6]. It has been reported that TMP can effectively promote the formation of primary twins ($\Sigma 3$ boundaries) and higher order twins ($\Sigma 9$ and $\Sigma 27$ boundaries), resulting in the occurrence of multiple-twinning [7-9]. Moreover, there are two main methods of TMP: a single cycle approach including single pre-straining and subsequent annealing for a long time at low temperature, and a multi-cycle approach including iterations of pre-straining followed by relatively

Received date: March 04, 2020

Foundation item: National Natural Science Foundation of China (51804187, 51904176); China Postdoctoral Science Foundation (2019M662400); Qingdao Post-doctoral Researcher Applied Research Programs; Key Technology Research and Development Program of Shandong (2019GGX104009)

Corresponding author: Zhou Haiping, Ph. D., Lecturer, College of Mechanical and Electronic Engineering, Shandong University of Science and Technology, Qingdao 266590, P. R. China, Tel: 0086-532-86057207, E-mail: zhouhp325@163.com

Copyright © 2020, Northwest Institute for Nonferrous Metal Research. Published by Science Press. All rights reserved.

high temperature annealing for a few minutes^[10].

In recent decades, some researchers have tried to improve the proportion of low- Σ CSL boundaries in Ni-based superalloy via optimized TMP schedules^[2, 3, 11-13]. Detrois et al^[11] optimized processing parameters of a single deformation anneal cycle for Ni-based superalloy RR1000, and the fraction of $\Sigma 3$ boundaries was increased to 52%. It was proposed that release of the strain energy upon annealing stimulates the formation of $\Sigma 3$ boundaries through strain induced boundary migration (SIBM). Li et al^[13] investigated the effect of deformation temperature and strain on the grain boundary character distribution of Inconel 600 alloy, and it was proposed that both the mechanisms of dynamic recrystallization and dynamic recovery might potentially be exploited to develop commercially viable processes for GBE of high performance alloys. Tan et al^[12] studied the effect of TMP on the grain boundary character distribution of Inconel 617 alloy, and the fractions of $\Sigma 3^n$ ($n=1, 2, 3$) boundaries significantly increase through TMP, reach about 5 times of that of the as-received sample. Xia et al^[2] investigated the feasibility of applying GBE to Alloy 690 tube for improving the intergranular corrosion resistance, and the fraction of low- Σ CSL boundaries was enhanced to about 75%, through small amount of deformation and subsequent short time annealing at high temperature. Meanwhile, large size grain-clusters form, inside which all the boundaries are $\Sigma 3^n$ type and lots of interconnected $\Sigma 3^n$ type triple junctions form. Bai et al^[13] studied the effects of TMP on the grain boundary character distribution evolution during high temperature annealing in alloy 825, and they found that GBE is achieved through recrystallization rather than grain growth. Although TMP is considered as an effective process to improve the fraction of low- Σ CSL boundaries for Ni-based superalloy, it also has some disadvantages. At present, the deformation strain in the TMP of Ni-based superalloy is relatively low, which restricts the dimension and complexity of components. In addition, the short annealing time may be incompatible with the great thermal inertia inherent in the large components^[11]. Besides that, the multi-cycle TMP will extend manufacturing time and add cost. Due to the aforementioned limitations, the current TMP approaches for GBE are not ideally suited for manufacturing the large and complex components made of Ni-based superalloy.

In addition, some models have also been proposed to understand the evolution of $\Sigma 3^n$ boundaries during GBE processing. Randle et al^[14, 15] proposed that $\Sigma 3$ boundaries arise from $\Sigma 3^n$ interactions, known as “ $\Sigma 3$ regeneration model”. Kumar et al^[16] thought that the formation of $\Sigma 3^n$

boundaries is mainly attributed to the decomposition of high energy boundary during GBE processing, which is termed as “boundary decomposition mechanism”. Wang et al^[17] proposed that the migration of incoherent $\Sigma 3$ boundaries in the recrystallized grains can play a significant role in the formation of $\Sigma 3^n$ boundaries. Xia et al^[13, 18] proposed that the increase in fraction of $\Sigma 3^n$ boundaries is mainly attributed to the formation of large grain-clusters, which is formed by multiple twinning during recrystallization. As can be seen from the previous researches, the grain boundary character distribution evolution during GBE processing is very complicated, and more research is still needed to understand the mechanism.

In this work, the effect of various TMP parameters on the grain boundary character distribution evolution in a typical Ni-based superalloy was researched, and the evolution mechanisms were also discussed in detail.

1 Experiment

The Ni-based superalloy used in this study was GH3030 alloy, and the chemical composition is listed in Table 1. Such alloy is a typical Ni-based superalloy used in the aerospace field, has excellent mechanical properties, long-term structure stability and well plasticity^[19]. During the experiment, the alloy was firstly solution-treated at 1130 °C for 2 h, followed by air cooling. After solution treatment, the samples were cold-rolled to the strains of 10%, 30%, 50% and 70%. And then, these rolled samples were subsequently annealed at 700, 800, 900 °C for 1~2 h. After annealing treatment, the samples were water-quenched immediately to preserve the high-temperature microstructure.

Electron backscatter diffraction (EBSD) was used to characterize the grain boundary character distribution of the studied alloy, using the HKL-Channel 5 system attached to a TESCAN MAIA 3 field emission gun scanning electron microscope (SEM). The samples for EBSD characterization were firstly ground with SiC papers, and the final polishing was finished through Ar ion milling technique. EBSD analysis was carried out in a rectangular analyzed area, with a step size of 0.5~1 μm . Any adjacent point pair with a misorientation exceeding 2° was considered as a boundary, and values of the fractions of grain boundaries in this investigation were expressed as length fractions. In addition, the CSL grain boundaries were categorized according to Brandon criterion of $\Delta\theta \leq 15^\circ \Sigma^{-1/2}$ ^[20]. The grain boundaries with $3 \leq \Sigma \leq 29$ were considered as low- Σ CSL boundaries, and grain boundaries with misorientation angles ranging

Table 1 Chemical composition of GH3030 alloy (wt%)

C	Cr	Ti	Al	Fe	Mn	Si	P	S	Ni
≤0.12	19. 0~22.0	0. 15~0.35	≤0.15	≤1.5	≤0.7	≤0.8	≤0.03	≤0.02	Bal.

from 2° to 15° were regarded as $\Sigma 1$ boundaries.

Moreover, transmission electron microscopy observation was performed by a JEM-200 EX transmission electron microscope (TEM). To prepare TEM foils, discs with 3 mm in diameter were punched from the samples after annealing treatments, and subsequently mechanically ground to a thickness of about 70 μm . And then, these thin-foil TEM specimens were twin-jet electropolished, using a solution of 10% perchloric acid in ethanol at -25°C .

2 Results and Discussion

2.1 Initial microstructure of studied alloy

Fig.1 shows the microstructure of the studied alloy after solution treatment. In the solution-treated condition, the studied alloy contains equiaxed grains with an average grain size of about 12.8 μm , as shown in Fig.1a. Meanwhile, there are some annealing twins in the microstructure, as marked with arrows. The twin-related boundaries ($\Sigma 3^n$) are analyzed by EBSD technique, and Fig.1b shows the OIM map of grain boundary distribution, in which the random boundaries, $\Sigma 1$ boundaries, $\Sigma 3$ boundaries, $\Sigma 9$ and $\Sigma 27$ boundaries are represented by the black, gray, red, blue and green lines, respectively. In addition, it can be seen that most $\Sigma 3^n$ boundaries are $\Sigma 3$ boundaries, and the fraction of $\Sigma 3$ boundaries is about 31.7%. Compared to $\Sigma 3$ boundaries, the fractions of $\Sigma 9$ and $\Sigma 27$ boundaries are much lower, only 2.98% and 1.62%, respectively. Moreover, the fraction of $\Sigma 3$ boundaries is about 5.1%.

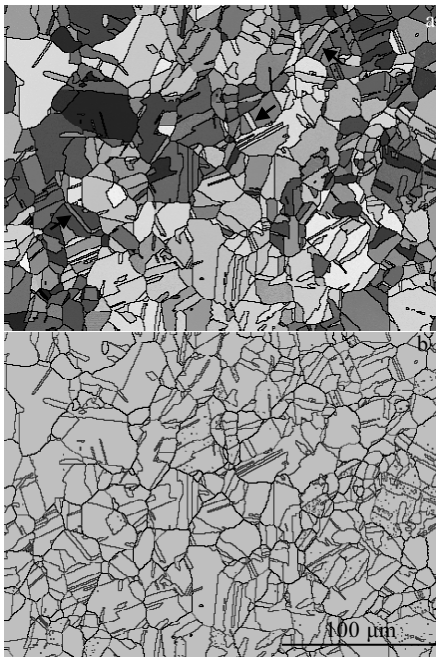


Fig.1 Initial microstructures of alloy after solution treatment: (a) IPF orientation map and (b) OIM map of grain boundary distribution

2.2 Effect of annealing time on microstructure evolution

Fig.2 shows the microstructures of the 50% cold-rolled alloy annealed at 700°C for different time. As shown in Fig.2a and 2b, the occurrence of static recrystallization (SRX) behavior can be clearly seen, and an inhomogeneous equiaxed grain structure is achieved. There are a large number of $\Sigma 1$ boundaries in the microstructure, most of which form during the cold rolling process. Few original $\Sigma 3$ boundaries can be seen in the deformed grains, due to the fact that the original $\Sigma 3$ boundaries will lose their orientation characteristics during cold rolling, caused by the rotation of grains [21]. Meanwhile, there are a lot of small SRX grains located at the boundaries of the deformed grains, and new $\Sigma 3$ boundaries form in these SRX grains. These $\Sigma 3$ boundaries mainly form by two mechanisms. The growth accident model is the first mechanism, which states that the formation of $\Sigma 3$ boundaries is attributed to the stacking sequence errors on $\{111\}$ planes during recrystallization process [22]. The migration of SRX grain boundaries can stimulate the formation of stacking errors, and some HAGBs can be partially transformed into $\Sigma 3$ boundaries [23]. The second mechanism is $\Sigma 3$ regeneration mechanism, which relies on the interactions of $\Sigma 3^n$ boundaries. Meanwhile, it has been reported that $\Sigma 3^n + \Sigma 3^{n+1} \rightarrow \Sigma 3$ occurs more frequently at triple junctions than $\Sigma 3^n + \Sigma 3^{n+1} \rightarrow \Sigma 3^{n+2}$ [14]. However, the triple junctions of $\Sigma 3$ - $\Sigma 3$ - $\Sigma 9$ and $\Sigma 3$ - $\Sigma 9$ - $\Sigma 27$ are very rare in Fig.2b, indicating the weakened interactions of $\Sigma 3^n$ boundaries. It can be inferred that growth accident model should be the main formation mechanism for these new $\Sigma 3$ boundaries in the SRX grains. Besides, $\Sigma 3$ boundaries can be divided into two types: coherent $\Sigma 3$ boundaries ($\Sigma 3_c$) and incoherent $\Sigma 3$ boundaries ($\Sigma 3_{ic}$). The interface energy of $\Sigma 3_c$ boundaries is much lower than that of $\Sigma 3_{ic}$ boundaries, owing to the perfect grain boundary atom arrangement of $\Sigma 3_c$ boundaries [6]. In addition, $\Sigma 3_c$ boundaries are featured by the morphology of straight lines, while $\Sigma 3_{ic}$ boundaries do not have such morphology. According to the morphology of $\Sigma 3$ boundaries in Fig.2b, many $\Sigma 3$ boundaries belong to $\Sigma 3_{ic}$ boundaries. Moreover, the high-density dislocations around the deformed grains are considered to be beneficial to the formation of $\Sigma 3_{ic}$ boundaries [15]. Compared to $\Sigma 3_c$ boundaries, $\Sigma 3_{ic}$ boundaries exhibit higher mobility, which are more likely to migrate and encounter other grain boundaries, leading to the interactions of $\Sigma 3^n$ boundaries.

With the increase of annealing time, the large deformed grains are gradually replaced by the small SRX grains, as shown in Fig.2c~2h. Although the fraction of SRX grains increases with the prolongation of annealing time, all of the grain structures are inhomogeneous at 700°C . Meanwhile, the fraction of $\Sigma 1$ boundaries is reduced gradually, and more $\Sigma 3$ boundaries form in the SRX grains with the

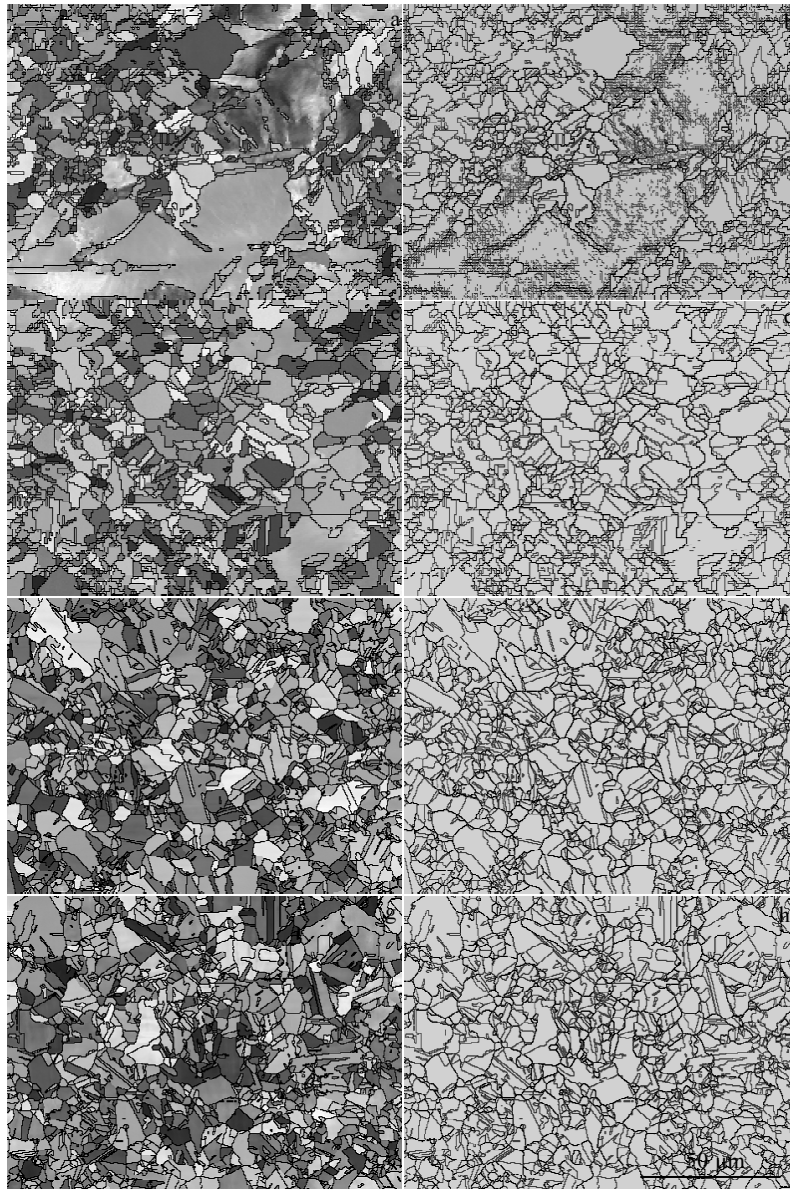


Fig.2 Microstructures of 50% cold-rolled alloy annealed at 700 °C for different time: (a, b) 0.5 h, (c, d) 1 h, (e, f) 1.5 h and (g, h) 2 h

annealing time. The distribution of $\Sigma 3$ boundaries is dependent on the fraction of SRX grains. In addition, more $\Sigma 3_c$ boundaries can be observed in the samples treated for a longer annealing time, and there are two main reasons for this phenomenon. The first reason is that more interfacial energy will be consumed by the occurrence of SRX behavior, and the formation of $\Sigma 3_{ic}$ boundaries will be inhibited, due to their large interfacial energy. The second reason is that $\Sigma 3_{ic}$ boundaries might be transformed into the stable $\Sigma 3_c$ boundaries with the prolongation of annealing time.

In order to further study the microstructure of the studied alloy during annealing treatment, TEM observation was carried out. As shown in Fig.3a, there are some new an-

nealing twins formed in the SRX structures, which ($\Sigma 3$ boundaries) are formed in the wake of migrating grain boundaries during SRX process. It has been reported that the high angle grain boundaries (HAGBs) in the cold-rolled alloy can be partially transformed into $\Sigma 3^n$ ($n=1, 2, 3$) boundaries through twin emission^[24]. The selected area electron diffraction (SAED) pattern taken from the twinning region is shown in Fig.3b. It should be noted that both the migration velocity and migration distance of grain boundaries are the key factors to the formation of $\Sigma 3$ boundaries during annealing treatment^[25]. Meanwhile, SRX grains nucleate along the prior HAGBs, and SRX behavior may occur through the grain boundary migration,

which will have a great influence on the formation of $\Sigma 3$ boundaries. Moreover, the interfacial energy of the cold-rolled alloy is consumed by twinning, which can promote the absorption of dislocations and mobility of grain boundaries during SRX process [15]. The occurrence of twinning will also stimulate the growth of SRX grains [26]. In other words, twinning may play an indirect role in the SRX behavior during annealing treatment.

Table 2 lists the grain boundary character distribution statistics and grain size for the samples of 50% cold-rolled alloy annealed at 700 °C for different time. It can be observed that the fraction of $\Sigma 3$ boundaries is much larger than that of $\Sigma 9$ and $\Sigma 27$ boundaries, which are no more than 4%. Such phenomenon also indicates that the $\Sigma 3$ boundaries are hardly formed via the interactions of $\Sigma 3^n$ boundaries. In addition, it can be clearly seen that the fraction of $\Sigma 1$ boundaries decreases with increasing the annealing time, while the fraction of $\Sigma 3$ boundaries exhibits the opposite trend, which changes slowly after annealing for more than 0.5 h. When the annealing time is 0.5 h, the fraction of $\Sigma 1$ boundaries reaches the highest value, 70.6%, while the fraction of $\Sigma 3$ boundaries and random boundaries is just only 12% and 14.1%, respectively. Such phenomenon is mainly attributed to the low fraction of SRX grains at annealing time of 0.5 h. With increasing the annealing time, there is more time for SRX grain boundary migration, which will stimulate the formation of $\Sigma 3$ boundaries by in-

creasing the frequency of growth accidents. In the sample annealed for 2 h, the fraction of $\Sigma 3$ boundaries reaches about 53%. Moreover, the fractions of $\Sigma 9$, $\Sigma 27$ and random boundaries exhibit the minimum values in the sample annealed for 0.5 h, which show little change after annealing for more than 0.5 h. In other words, $\Sigma 9$ and $\Sigma 27$ boundaries are very difficult to form in large quantities via interactions of $\Sigma 3^n$ boundaries with increasing the annealing time at 700 °C. Besides, it can also be found that the average grain size decreases slightly with increasing the annealing time, which is closely related to the increase of fraction of SRX grains. As SRX behavior and grain refinement occur during annealing treatment, the formation of new SRX grains creates $\Sigma 3$ boundaries and increases their overall length.

2.3 Effect of annealing temperature on microstructure evolution

In order to avoid obvious grain coarsening after long time annealing treatment, according to the fraction of $\Sigma 3$ boundaries in the alloy annealed at 700 °C for different time, the samples annealed for 1 h were chosen as objects to study the effect of annealing temperature on microstructure evolution of the studied alloy. Fig.4 shows the microstructures of the 50% cold-rolled alloy annealed at different temperatures for 1 h. From Fig.2c, Fig.4a and 4c, it can be found that there are still some deformed grains in the sample annealed at 700 and 800 °C, while full recrystallization is achieved at the temperature of 900 °C. Such phenomenon

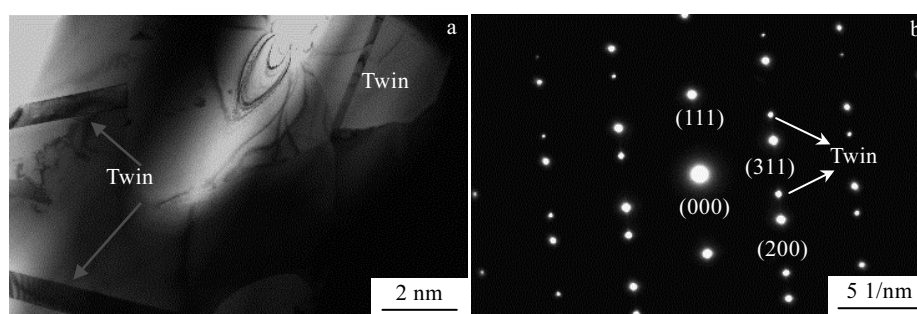


Fig.3 TEM image (a) and SAED pattern (b) of 50% cold-rolled alloy annealed at 700 °C for 1 h

Table 2 Grain boundary character distribution statistics and grain size of 50% cold-rolled alloy annealed at 700 °C for different time

Annealing time/h	0.5	1	1.5	2
$\Sigma 1$ /%	70.6	12.5	5.2	4
$\Sigma 3$ /%	12	42.6	51.8	53
$\Sigma 9$ /%	1.2	4	3.7	3.8
$\Sigma 27$ /%	0.4	1.5	1.8	1.7
Random boundary/%	14.1	38.9	36.1	35.3
Average grain size/ μm	6.3	5.1	4.5	4.39

indicates that the SRX process is accelerated at higher annealing temperature, which is mainly attributed to the higher mobility of grain boundaries at higher temperatures. As shown in Fig.4b and 4d, very few $\Sigma 1$ boundaries can be observed, and a lot of new $\Sigma 3$ boundaries form in the SRX grains. Meanwhile, the distribution of $\Sigma 3$ boundaries is very uniform in the sample annealed at 900 °C, owing to the occurrence of full recrystallization. Moreover, the annihilation of defects may lead to recovery of pre-existing twin boundaries, which are partly destroyed during rolling deformation [27]. Besides, due to the fact that the stored energy is mostly consumed by recrystallization during the annealing treatment, only few $\Sigma 3$ - $\Sigma 3$ - $\Sigma 9$ and $\Sigma 3$ - $\Sigma 9$ - $\Sigma 27$ triple

junctions form. In addition, some curved Σ_{3ic} boundaries can also be observed in these samples, which might be formed via growth accident during the process of HAGBs migration.

Table 3 lists the grain boundary character distribution statistics and grain size for the samples of 50% cold-rolled alloy annealed at different temperatures for 1 h. It can be found that both $\Sigma 1$ boundaries and random boundaries exhibit the highest fraction at 700 °C, and very few $\Sigma 1$ boundaries are left at the temperature higher than 800 °C. On the contrary, the fraction of $\Sigma 3$ boundaries increases with increasing the annealing temperature, which reaches above 50% at the temperatures higher than 800 °C. Such phenomenon is mainly attributed to the faster grain boundary migration at the higher annealing temperature, which can stimulate the occurrence of growth accidents. Meanwhile, it might be easier for random boundaries to transform into $\Sigma 3$ boundaries through twin emission at the higher temperature.

In addition, it should be noted that the fraction of $\Sigma 3$

boundaries increases very slowly, when the annealing temperature is higher than 800 °C. This is due to the fact that both the fraction of SRX grains and grain size can influence the grain boundary character distribution evolution. Firstly, it is very close to full recrystallization at the temperature higher than 800 °C, so the fraction of $\Sigma 3$ boundaries increases slowly to the peak value. Secondly, it can be found that the average grain size increases with increasing the annealing temperature, as listed in Table 3. It has been reported that the small grains can be consumed by large grains, and grow without producing new $\Sigma 3$ boundaries during the grain growth stage after recrystallization^[28]. In a word, the grain growth during annealing treatment may be unfavorable to further increase the fraction of $\Sigma 3$ boundaries. In addition, the fraction of $\Sigma 9$ and $\Sigma 27$ boundaries is below 4.2%, and its variation is also very small with increasing the temperature. Compared to $\Sigma 3$ boundaries, the annealing temperature has less effect on the fraction of $\Sigma 9$ and $\Sigma 27$ boundaries, which is mainly due to the weakened interaction between different $\Sigma 3^n$ boundaries.

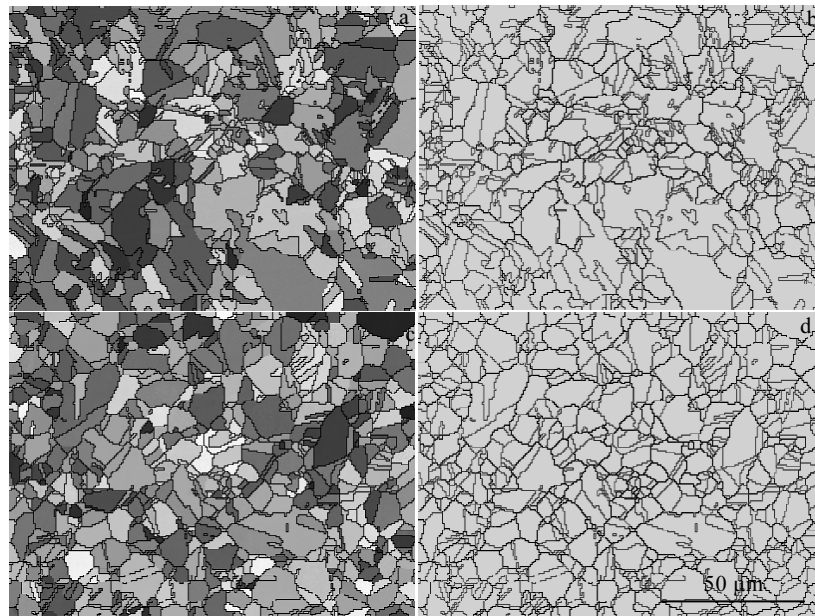


Fig.4 Microstructures of 50% cold-rolled alloy annealed at 800 °C (a, b) and 900 °C (c, d) for 1 h

Table 3 Grain boundary character distribution statistics and grain size of 50% cold-rolled alloy annealed at different temperatures for 1 h

Temperature/°C	700	800	900
$\Sigma 1/\%$	12.5	4.8	3.6
$\Sigma 3/\%$	42.6	50.6	51.5
$\Sigma 9/\%$	4	4.2	3.8
$\Sigma 27/\%$	1.5	1.6	1.5
Random boundary/%	38.9	35.7	35.9
Average grain size/ μm	5.1	7.02	7.52

2.4 Effect of cold-rolling strain on microstructure evolution

Fig.5 shows the microstructures of the cold-rolled alloy annealed at 900 °C for 1 h with different deformation strains. At the small strain of 0.1, the obvious grain growth can be clearly seen, as shown in Fig.5a. The low stored energy in the cold-rolled alloy with small strain will lead to the low density of SRX nuclei during the annealing treatment, which have large potential space to grow through consuming the deformed area. Meanwhile, some large grain-clusters can be clearly seen in Fig.5b, in which there are a few $\Sigma 3$ - $\Sigma 3$ - $\Sigma 9$ or $\Sigma 3$ - $\Sigma 9$ - $\Sigma 27$ triple junctions, as marked by the circles. The

grain-clusters are surrounded by HAGBs and contain a high fraction of low- Σ CSL grain boundaries, which are also known as twin-related domains (TRD) [8]. It has been reported that the formation of grain-clusters begins from a single SRX nucleus during recrystallization, which will generate a series of $\Sigma 3$ annealing twin boundaries, and form the interconnected $\Sigma 3^n$ type grain boundaries [29]. Meanwhile, in these grain-clusters, any two grains have a $\Sigma 3^n$ mutual misorientation relationship no matter whether they are adjacent. With increasing the deformation strain, the large deformed grains are replaced by the small SRX grains, as shown in Fig.5c and 5d. Many new $\Sigma 3$ boundaries form in these SRX grains, and TRD size decreases with the grain refinement. When the strain increases to 0.7, the obvious growth of SRX grains can be observed, and as a result, TRD size also increases, as shown in Fig.5e and 5f. It is well known that the mobility of grain boundaries is governed by the stored energy and thermal driving forces [17]. During subsequent annealing process, the high stored energy in the cold-rolled alloy with large strain of 0.7 can significantly promote the mobility of grain boundaries, leading to the coarsening of SRX grains. As shown in Fig.5f, it can also be

found that most $\Sigma 3$ boundaries are $\Sigma 3_c$ boundaries. At the large strain of 0.7, most of the interface energy will be consumed by the rapid growth of SRX grains, which is less energetically favorable for the formation of $\Sigma 3_{ic}$ boundaries. On the contrary, $\Sigma 3_c$ boundaries will be easy to form at the large strain of 0.7, owing to their low interface energy.

Table 4 lists the grain boundary character distribution statistics and grain size for the samples of cold-rolled alloy annealed at 900 °C for 1 h with different strains. It can be clearly seen that there are very few $\Sigma 1$ boundaries left in the samples with the strain larger than 0.5, while the random boundaries reach the lowest fraction at the strain of 0.1. Interestingly, the fraction of the random boundaries is inversely proportional to the average grain size.

In addition, the fraction of $\Sigma 3^n$ ($n=1, 2, 3$) boundaries decreases firstly, and then increases with increasing the strain. At the small strain of 0.1, the fraction of $\Sigma 3$ boundaries reaches about 62.7%, which is closely related to the formation of large grain-clusters. The development of grain-clusters during recrystallization will lead to the formation of $\Sigma 3$ boundaries behind the front of migrated grain boundary [22]. Moreover, the fractions of $\Sigma 9$ and $\Sigma 27$ boundaries reach the maximum value at

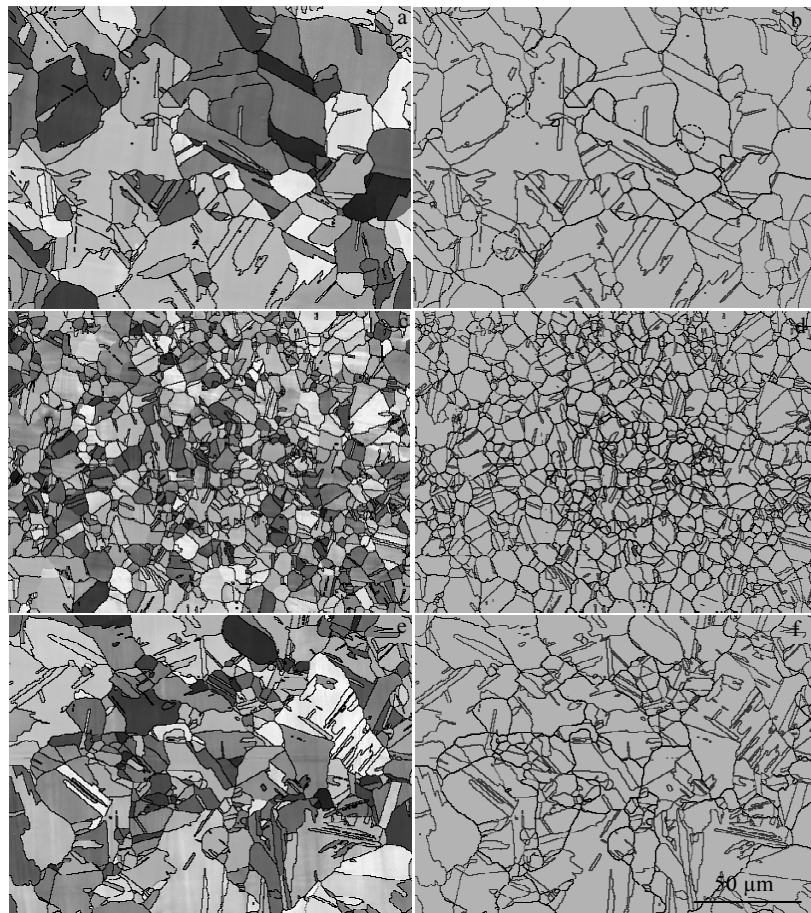


Fig.5 Microstructures of cold-rolled alloy annealed at 900 °C for 1 h with different deformation strains: (a, b) 0.1, (c, d) 0.3, and (e, f) 0.7

Table 4 Grain boundary character distribution statistics and grain size of cold-rolled alloy annealed at 900 °C for 1 h with different deformation strains

Strain	0.1	0.3	0.5	0.7
$\Sigma 1/\%$	10.4	24	3.6	3.8
$\Sigma 3/\%$	62.7	36.4	51.5	59.9
$\Sigma 9/\%$	5.7	1.1	3.8	4.3
$\Sigma 27/\%$	3.7	0.6	1.5	2.1
Random boundaries/ $\%$	16.6	37.6	35.9	28.5
Average grain size/ μm	15.6	6.1	7.52	11.6

the small strain of 0.1, which is mainly due to the strengthened interaction of $\Sigma 3^n$ grain boundaries in the large grain-clusters. It has also been reported that $\Sigma 9$ and $\Sigma 27$ boundaries form, when two separate grain boundary fronts of the grain-cluster impinge upon each other [22]. At the strain of 0.3, the fractions of $\Sigma 3^n$ ($n=1, 2, 3$) boundaries exhibit the minimum value, which is mainly attributed to the low fraction of SRX grains. With increasing the strain, the fraction of $\Sigma 3$ boundaries increases, which can almost reach 60% at the large strain of 0.7. The development of $\Sigma 3$ boundaries depends on grain boundary migration, which will be promoted by the high stored energy induced by the large deformation. In addition, the fractions of $\Sigma 3$ boundaries are very high at the strains of 0.1 and 0.7, which are also closely related to the large TRD size, as shown in Fig.5. It has been reported that there is a correlation between the TRD size and the overall twin boundary fraction, while the twin fraction initially rises rapidly before eventually plateaus with increasing the TRD size [30]. In other words, the growing grain-clusters are beneficial for the formation of $\Sigma 3$ boundaries. Besides, the change trend of the fractions of $\Sigma 9$ and $\Sigma 27$ is almost the same as that of $\Sigma 3$ boundaries, mainly due to the interaction of $\Sigma 3^n$ boundaries during annealing treatment.

3 Conclusions

1) During the annealing treatment, growth accident model is the main mechanism for the formation of new $\Sigma 3$ boundaries in the SRX grains, while the migration of SRX grain boundaries can also promote the formation of stacking errors. With increasing the annealing time, there is more time for SRX grain boundary migration, which stimulates the formation of $\Sigma 3$ boundaries by increasing the frequency of growth accidents. Meanwhile, there are more $\Sigma 3_c$ boundaries in the samples annealed for a longer time.

2) The fraction of $\Sigma 3$ boundaries increases with increasing the temperature, which is mainly due to the faster migration of grain boundaries at higher annealing temperatures. In addition, the fraction of $\Sigma 3$ boundaries decreases

firstly, and then increases with increasing the strain. At strains of 0.1 and 0.7, the fractions of $\Sigma 3$ boundaries reach around 60%, which is related to the well development of large grain-clusters. In addition, although the fractions of $\Sigma 9$ and $\Sigma 27$ are very small, their changing trend under different TMP parameters is similar to that of $\Sigma 3$ boundaries, which is mainly due to the interaction of $\Sigma 3^n$ boundaries during annealing treatment.

References

- Pradhan S, Mandal S, Athreya C et al. *Materials Science and Engineering A* [J], 2017, 700: 49
- Xia S, Li H, Liu T G et al. *Journal of Nuclear Materials*[J], 2011, 416(3): 303
- Li B, Tin S. *Materials Science and Engineering A*[J], 2014, 603: 104
- Kumar S, Prasad B S, Kain V et al. *Corrosion Science*[J], 2013, 70: 55
- Telang A, Gill A S, Tammana D et al. *Materials Science and Engineering A*[J], 2015, 648: 280
- Randle V, Coleman M. *Acta Materialia*[J], 2009, 57(11): 3410
- Liu T, Xia S, Wang B et al. *Materials & Design*[J], 2016, 112: 442
- Cayron C. *Acta Materialia*[J], 2011, 59(1): 252
- Gertsman V Y, Henager C H. *Interface Science*[J], 2003, 11(4): 403
- Li Q, Guyot B, Richards N. *Materials Science and Engineering A*[J], 2007, 458(1-2): 58
- Detroit M, Rotella J, Goetz R L et al. *Materials Science and Engineering A*[J], 2015, 627: 95
- Tan L, Sridharan K, Allen T. *Journal of Nuclear Materials*[J], 2007, 371(1-3): 171
- Bai Q, Zhao Q, Xia S et al. *Materials Characterization*[J], 2017, 123: 178
- Randle V, Owen G. *Acta Materialia*[J], 2006, 54(7): 1777
- Randle V. *Acta Materialia*[J], 2004, 52(14): 4067
- Kumar M, Schwartz A J, King W E. *Acta Materialia*[J], 2002, 50(10): 2599
- Wang W, Guo H. *Materials Science and Engineering A*[J], 2007, 445: 155
- Xia S, Zhou B, Chen W. *Metallurgical and Materials Transactions A*[J], 2009, 40(12): 3016
- Zhan T, Chai F, Zhao J et al. *Journal of Mechanical Science and Technology* [J], 2018, 32(6): 2613
- Brandon D. *Acta Metallurgica*[J], 1966, 14(11): 1479
- Zhang H, Zhang K, Jiang S et al. *Journal of Alloys and*

- Compounds[J], 2015, 623: 374
- 22 Barr C M, Leff A C, Demott R W et al. *Acta Materialia*[J], 2018, 144: 281
- 23 Zhang H, Zhou H, Qin S et al. *Materials Science and Engineering A*[J], 2017, 696: 290
- 24 Wang K, Wei A, Tong X et al. *Materials Letters*[J], 2018, 211: 118
- 25 Mahajan S, Pande C, Imam M et al. *Acta Materialia*[J], 1997, 45(6): 2633
- 26 Field D, Bradford L, Nowell M et al. *Acta Materialia*[J], 2007, 55(12): 4233
- 27 Bozzolo N, Souaï N, Logé R E. *Acta Materialia*[J], 2012, 60(13-14): 5056
- 28 Jin Y, Lin B, Bernacki M et al. *Materials Science and Engineering A*[J], 2014, 597: 295
- 29 Liu T, Xia S, Li H et al. *Materials Letters*[J], 2014, 133: 97
- 30 Bober D B, Lind J, Mulay R P et al. *Acta Materialia*[J], 2017, 129: 500

形变热处理工艺参数对冷轧态镍基高温合金晶界特征分布演变的影响

张弘斌¹, 周海萍¹, 张成才¹, 韩宝坤¹, 高魁东¹, 李辉平¹, 秦升学¹, 刘杰¹, 王艳¹, 张鹏²

(1. 山东科技大学, 山东 青岛 266590)

(2. 抚顺特钢股份有限公司, 辽宁 抚顺 113000)

摘要: 研究了不同形变热处理工艺参数对冷轧态镍基高温合金中晶界特征分布演变的影响。结果表明, 在退火处理过程中, 生长事故模型是静态再结晶(SRX)晶粒中新 $\Sigma 3$ 晶界形成的主要机制。随着退火时间和退火温度的增加, 晶界迁移时间延长, 晶界迁移速度加快, 从而增加了生长事故的发生频率, 促进了 $\Sigma 3$ 晶界的形成。此外, 随着应变的增加, $\Sigma 3$ 晶界的比例先减小后增大。在冷轧变形量为0.1和0.7时, $\Sigma 3$ 晶界的比例均可达到60%左右, 这与大晶粒团簇的形成密切相关。此外, 分析了不同工艺参数下, $\Sigma 1$ 晶界、共格 $\Sigma 3$ 晶界、非共格 $\Sigma 3$ 晶界、 $\Sigma 9$ 晶界、 $\Sigma 27$ 晶界和随机晶界的演变规律。

关键词: 镍基高温合金; 晶界特征分布; CSL晶界; 形变热处理工艺

作者简介: 张弘斌, 男, 1985年生, 博士, 讲师, 山东科技大学机械电子工程学院, 山东 青岛 266590, 电话: 0532-86057207, E-mail: skzhanghongbin@163.com